ELSEVIER

Journal of Nuclear Materials 283–287 (2000) 120–127

journal of nuclear materials

www.elsevier.nl/locate/jnucmat

A cleavage toughness master curve model

G.R. Odette *, M.Y. He

Department of Mechanical and Environmental Engineering, University of California, Santa Barbara, CA 93106-5070, USA

Abstract

Development of fusion power will require a fracture toughness database, derived largely from small specimen tests, closely integrated with methods to assess first wall and blanket structural integrities. A master curve-shift (MC–ΔT) method has been proposed as an engineering expedient to treat the effects of structural geometry, irradiation, loading rates and safety margins. However, a number of issues related to the MC–ΔT method remain to be resolved, including the universality of MC shapes. A new micromechanical model of fracture toughness in the cleavage transition regime is proposed that combines analytical representations of finite element analysis simulations of crack-tip stress fields with a local critical stress-critical stressed area (σ^*–A^*) fracture criterion. This model, has been successful in predicting geometry effects, as well as high loading rate and irradiation hardening-induced Charpy shifts. By incorporating a modest temperature dependence in $\sigma^*(T)$, an inconsistency between model predictions and an observed universal-type MC shape is resolved.

1. Introduction – the master curve-shift method

Design and operation of defect tolerant fusion structures will require a fracture toughness database and methods to apply this information in integrity assessment [1]. We define fracture toughness as the property, or properties, that specify the fracture load (P_f) and displacement (Δ_f) which cause an extension of a sharp Mode I fatigue crack. The actual $P-\Delta$ experienced by a structure must maintain a safe margin, including under start-up/shut-down and off-normal transient conditions. Engineering designs also usually demand some degree of plastic ductility prior to failure.

The $P_f-\Delta_f$ depend on extrinsic factors such as temperature (T), loading rate (P') and the size and geometry of the cracked body. Intrinsic fracture toughness of a material is governed by its type, crystal structure and microstructure, starting in the as-fabricated state, and evolving in-service, due to factors such as exposure to neutrons (ϕt). Typically, in-service conditions degrade toughness. Fracture toughness generally cannot be described by a single material property [1]. However, we will use the concept of an effective toughness (K_e), which can be measured in laboratory-scale tests (predominantly using small specimens), and applied to estimate the $P_f-\Delta_f$ for complex structures.

Fig. 1 illustrates the effects of size and geometry on 3-D finite element calculations (using ABAQUS) of P vs Δ curves for a three-point bending geometry with a crack depth (a) and span (S)-to-width (W) ratios of $a/W=0.5$ and $S/W=4$ for various W and thickness (B) values.In all cases the curves are terminated when the elasto-plastic loading (K_J) averaged across the crack front reaches 100 MPa $\sqrt{m}$ (P_{100},Δ_{100}). The P and Δ are normalized by the nominal plane strain limit load (P_L) and the Δ at the $P_L(\Delta_L)$, respectively. In the case of the $B/W=5$, $W=2$ mm panel (solid line), lateral plane strain constraint is maintained with gross yielding at $P\cong P_L$ owing to the large B. The Δ_{100} is large (high ductility), due to the small b ($=W-a$). Loss of in-plane constraint in this case would result in an even larger Δ at fracture of a material with a small-scale yielding toughness of 100 MPa $\sqrt{m}$. In stark contrast, the filled circle marks the $K_J=100$ MPa $\sqrt{m}$ point in the fully elastic, brittle fracture regime ($P_{100}\ll P_L,\Delta_{100}<\Delta_L$) for a plate with $B/W=5$, $W=140$ mm. In the case of a typical specimen geometry, with $B/W=0.5$ and $W=10$ mm (dashed line), $K_J=100$ MPa $\sqrt{m}$ is reached after a small amount of plastic deformation; yielding starts at

* Corresponding author. Tel.: +1-805 893 3525; fax: +1-805 893 8651.

E-mail address: odette@engineering.ucsb.edu (G.R. Odette).

0022-3115/00/$ - see front matter
PII: S0022-3115(00)00334-2

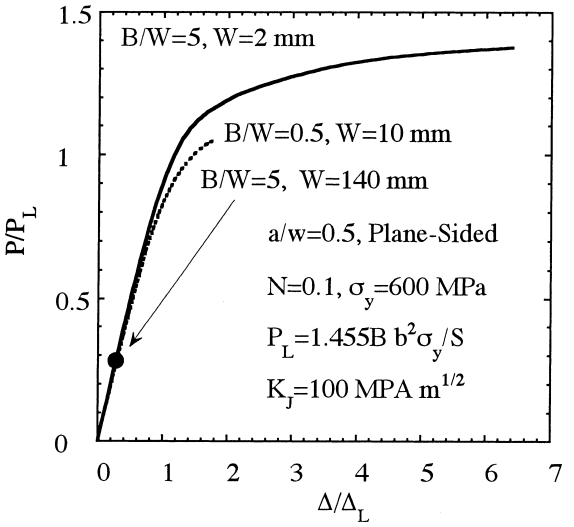

Fig. 1. Normalized load–displacement curves for different cracked body geometry for a common $K_{Jc} = 100$ MPa $\sqrt{m}$.

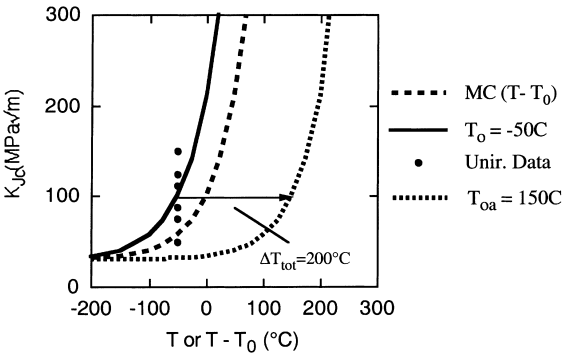

Fig. 2. Illustration of the MC–ΔT method.

$P < P_L$ indicating some loss of lateral constraint. These results illustrate that a thin fusion structure may be effectively ductile even when a heavy-section pressure vessel structure, with the same material toughness, is extremely brittle.

A MC–ΔT method has been proposed as a possible practical approach to deal with the enormous amount of information that is needed to characterize and apply toughness [2]. While significantly different in detail and philosophy, this method extends from the revolutionary MC technology developed for treating cleavage fracture in the transition for applications to reactor pressure vessels (RPV) and other large thick-walled structures [3]. The MC–ΔT method assumes a universal toughness $K_{mc}(T - T_0)$ curve shape can be placed (indexed) on an absolute temperature (T) scale by a reference temperature (T_0) at a reference toughness (e.g., 100 MPa $\sqrt{m}$). Typically, T_0 would be determined by standard K_{Jc} measurements on an unirradiated alloy. The T_0 is then adjusted (T_{oa}) by a set of temperature shifts (ΔT) that account for the effects of loading rate (P'), irradiation (ϕt), size and geometry factors (g), and a safety margin (m) $T_{oa} = T_0 + \Delta T_{P'} + \Delta T_{\phi t} + \Delta T_g + \Delta T_m$ [2].

The MC–ΔT method is illustrated in Fig. 2. The static MC deep crack shape is shown as the dashed line plotted on a $T - T_0$ scale. The solid line is the corresponding reference (unirradiated) MC placed on an absolute temperature scale, at $T_0 = -50$°C at $K_{Jc} = 100$ MPa $\sqrt{m}$, by the six tests shown as filled circles. A net shift of 200°C, arising from irradiation ($\Delta T_{\phi t} = 150$°C), dynamic loading ($\Delta T_{P'} = 50$°C), a thin-walled, shallow crack geometry ($\Delta T_g = -40$) and a margin ($\Delta T_m = 40$°C), places the absolute MC, used for structural evaluations, at $T_{oa} =$ 150°C, shown as the dotted line. Ideally, there would be only a single MC shape applicable to all conditions. While, in practice this is not the case, a small family of MC shapes may be sufficient for most practical applications [2].

The enormous benefit of the MC–ΔT approach is that:

- The $K_e(T)$ curves can be established with a relatively small number of tests on relatively small specimens.
- Independently established shifts and a small set of MC shapes account for the effects of other key variables.

Open questions about the MC–ΔT method include:

- Is there a universal MC shape, or small set of shapes, and if so why?
- Is the total shift equal to the sum of the various ΔTs?
- How should the large inherent statistical scatter in the transition be treated?
- How should explicit effects of size and geometry, in both testing and structural applications, be treated?
- How can T_0 and the ΔTs be modeled, both as a basis for improved alloys and to characterize effects of irradiation, including helium?

These issues can only be resolved by a good physical understanding of the underlying fracture mechanisms and mechanics. This study will focus on the issue of a universal MC shape.

2. A macro–micromechanics model of cleavage intitiation in the transition

It is generally accepted that cleavage fracture involves stress-controlled fracture of brittle 'trigger' particles (i.e., large grain boundary carbides) and subsequent dynamic microcleavage crack propagation into the tougher metal matrix [1,2,4]. These microfracture events require high local tensile (σ_{22}) stresses (of the order of 2000 MPa), far in excess of the uniaxial yield stress (σ_y), that occur in the concentrated tri-axial stress–

strain fields near a blunting macroscopic crack tip. Models of cleavage toughness combine simulations of the crack-tip stress fields with local micromechanical models of the field conditions required to initiate cleavage. For small-scale yielding (SSY), the fields are spatially self-similar functions of the angle from the crack plane and the distance from the crack tip (r) normalized by the crack-tip opening displacement (δ). Hence, $\sigma_{22}(r/\delta)/\sigma_y$ is independent of K_J and geometry [1]. The fields depend on strain hardening, typically represented by a power-law exponent (n), and, weakly, on σ_y/E, where E is the elastic modulus. The crack-tip fields can be computed using a finite element analysis (FEA) code for any specified constitutive law and geometry [2,5–7].

A number of micromechanical models have been used to describe the critical local stress field condition for cleavage, beginning with a critical-stress (σ^*) critical-distance (λ^*) criterion proposed by Ritchie et al. (RKR) [4]. For SSY, the σ_{22} is constant at a given r/δ. Thus as δ increases, r at $\sigma_{22} = \sigma^*$ increases. At $r(\sigma^*) = \lambda^*$, $\delta = \delta_{Ic}$ and cleavage occurs. The δ_{Ic} is related to toughness as $K_{Jc} = (m\delta_{Ic}\sigma_y E')^{1/2}$, where m ($\cong 2$) which depends on the geometry and the constitutive law, and can be computed using the FEA simulations [1,5]. An extension of the RKR model assumes cleavage occurs when a σ^* contour envelops a critical area (A^*) in front of the crack [2,5–7]. Other progenies of the RKR model are based on the weakest link statistics and critically stressed volume criteria [8–12]. Within this model framework, the σ^*–A^* are the basic local fracture properties that can be used along with the constitutive law, stress as a function of strain $\sigma(\varepsilon)$, to compute K_{Jc} for SSY; and, more generally, K_e for conditions that do not involve SSY constraint (e.g., small specimens, shallow and/or surface cracks).

The σ^* is the tensile stress needed to propagate a dynamic microcrack from a broken trigger particle and is usually given by a Griffith-type criteria [13,14]

$$\sigma^* = C_{tp}K_{micro}/\sqrt{d_{tp}}, \tag{1}$$

where C_{tp} is a geometric constant, K_{micro} the microarrest toughness of the metal matrix and d_{tp} is a characteristic dimension of the trigger particle. The critical area, A^*, is also mediated by the microstructure and by the necessity that the σ^* contour envelop a sufficient population of potential trigger particles. The σ^*–A^* represent a mean K_{Jc}, which is inherently scattered in the transition. Statistically, the probability of fracture increases from very low values at $A < A^*$ to unity as $A > A^*$. Based primarily on blunt notch tests and the coarse-scale (μm) of the trigger particle microstructures, a typical assumption has been that σ^*–A^* are independent of temperature, strain rate and, in many cases, irradiation exposure [2,7,8,13–15].

As proposed by Nevalainen and Dodds [5], for SSY the self-similar stress fields can be analytically represented in terms of the stressed area (A) within a specified normalized stress contour ($R = \sigma_{22}/\sigma_y$):

$$A = 10^{P(R)}\left[K_J/\sigma_y\right]^4. \tag{2a}$$

The ABAQUS FEA code was used to compute the $P(R)$ function based on a specified constitutive law for a three-point bend geometry with $a/W = 0.5$. The 2-D half symmetry mesh was composed of 4368 four-node plane strain bilinear elements with 4519 nodes. The mesh was highly refined near the crack tip and the smallest elements were less than one tenth of the initial radius of $0.002a$. A report on the detailed procedures and catalog of results is under preparation. However, the most salient result is that the FEA computations can be represented by a simple polynomial,

$$P = C_0 + C_1R + C_2R^2. \tag{2b}$$

The C_i are fitted to the detailed computational results. Thus from Eq. (2a),

$$K_{Jc} = \sigma_y\left[A^*10^{-P^*}\right]^{1/4}, \tag{2c}$$

where $P^* = P(R^* = \sigma^*/\sigma_y)$. By substituting appropriate values of σ^* and $\sigma_y(T)$ (thus defining R^*, hence, P^*) and A^* in Eqs. (2b) and (2c), $K_{Jc}(T)$ can be directly computed. This deterministic relation is strictly valid only in a temperature range where $\sigma_{22\,max} \geqslant \sigma^*$; nominally cleavage cannot occur above this temperature, giving way to ductile fracture. However, the K_{Jc} can be extrapolated to somewhat higher values, since σ^*–A^* actually has a statistical range of values that can be described by a $\sigma^*(A^*)$ function, with decreasing σ^* with increasing A^*. Statistical variations in σ^*–A^* also result in large K_{Jc} scatter in the transition.

The σ^*–A^* model is oversimplified for a number of other reasons. For example, macrocleavage is often preceded by the formation and arrest of a distributed population of facet-sized microcleavage cracks [2,6]. In this case, macroscopic fracture (or, in extreme cases, the so-called quasi-cleavage) results from the coalescence and instability of the damage in the process zone region [6]. Further, values of ferrite microcrack arrest toughness (K_{micro}) estimated from σ^* and d_{tp} are typically 3–10 or more times than that predicted by the Griffith theory for brittle fracture (e.g., >2.5 vs 0.9 MPa $\sqrt{m}$ for a nominal surface energy of 2 J/m^2) [13, 14]. Nevertheless the σ^*–A^* models have been highly successful in rationalizing a number of experimental observations, including:

- The general shape of the $K_{Jc}(T)$ curve at *low* T_0 [2,6].
- Temperature shifts in Charpy energy-temperature curves [18] and, up to some point, $K_{Jc}(T)$ curves [2,15], due to σ_y increases arising from both high strain (loading) rates and irradiation.

- Size and geometry mediated increases in $K_e > K_{Jc}$ arising from the loss of SSY constraint ($\sigma_{22} < \sigma_{22ssy}$) associated with lower notch acuity, shallow cracks (and the presence of so-called T-fields) or large-scale plasticity [2,5–7].

As noted previously, the constraint effects associated with deviations from SSY can also be evaluated using large deformation FEA simulations [2,5–7]. This requires determining the K_e/K_{Jc} (> 1) required to produce the same stressed area A for a given σ^*. The K_e/K_{Jc} is a function of R^*, the constitutive law, the cracked body geometry and the deformation level ($D = K_e^2/(W-a)E\sigma_y$). The results are from 3-D ABAQUS FEA simulations of three-point bend specimens with $a/W = 0.5$. The one-quarter symmetry mesh was composed of 2480 20-node quadratic brick elements with 11 889 nodes. Wedge-shaped nodes were used at the crack tip to efficiently model blunting. The results are for a strain-hardening exponent of $n = 0.1$ (see Eq. (4)). The A and K_J were averaged across the crack front. A report on the detailed procedures and catalog of results is also under preparation. Once again, however, the most salient result is that these FEA computations can also be analytically fit with simple polynomial expressions in the form [5]

$$K_e/K_{Jc} = \left[C_{c0} + C_{c1}R^* + C_{c2}R^{*2}\right]^{1/2}, \tag{3a}$$

where the C_{ci} coefficients depend on D as

$$C_{ci} = C_{ri0} + C_{ri1}D + C_{ri2}D^2. \tag{3b}$$

While they are very simple in form, Eqs. (2a)–(2c) and (3a) and (3b) represent a comprehensive physical model of effective fracture toughness in the transition region. This model can, in principle, account for all key factors that control the critical $P_f - \Delta_f$ cleavage conditions for a cracked body (test specimen or structure) including:

- The basic material constitutive behavior, $\sigma(\varepsilon, \varepsilon', T, \phi t)$, and local fracture properties, σ^*–A^*, as a function of strain rates (ε' or P'), temperature and microstructure.
- The size and geometry of the cracked body.
- Other effects not discussed here such as inherent statistical scatter and associated bounding limits and weakest link statistical geometry effects associated with the crack front length.

Fig. 3(a) shows the predicted $K_{Jc}(T)$ shape (solid line) from Eq. (2a)–(2c) for: (a) a Ramberg–Osgood constitutive law, given in Eq. (4), with $\varepsilon_\lambda = \varepsilon_y$; (b) a strain hardening exponent (n) of 0.1 and $\sigma_y(T)$ from a polynomial fit to RPV steel data; (c) $A^* = 10^{-8}$ m^2 and $\sigma^* = 2080$ MPa. The prediction is compared to the RPV steel MC with a T_0 at 100 MPa $\sqrt{m}$ of about −45°C (dashed line). The corresponding $K_e(T)$, curve for a small $3.3 \times 3.3 \times 16.6$ mm^3 1/3-sized bend specimen, tested well beyond the SSY limit, is shown as the other solid line shifted to lower temperatures by about −40°C. This smaller specimen $K_e(T)$ also compares favorably to the RPV MC shape with T_0 shifted to about −85°C (also shown as a dashed line).

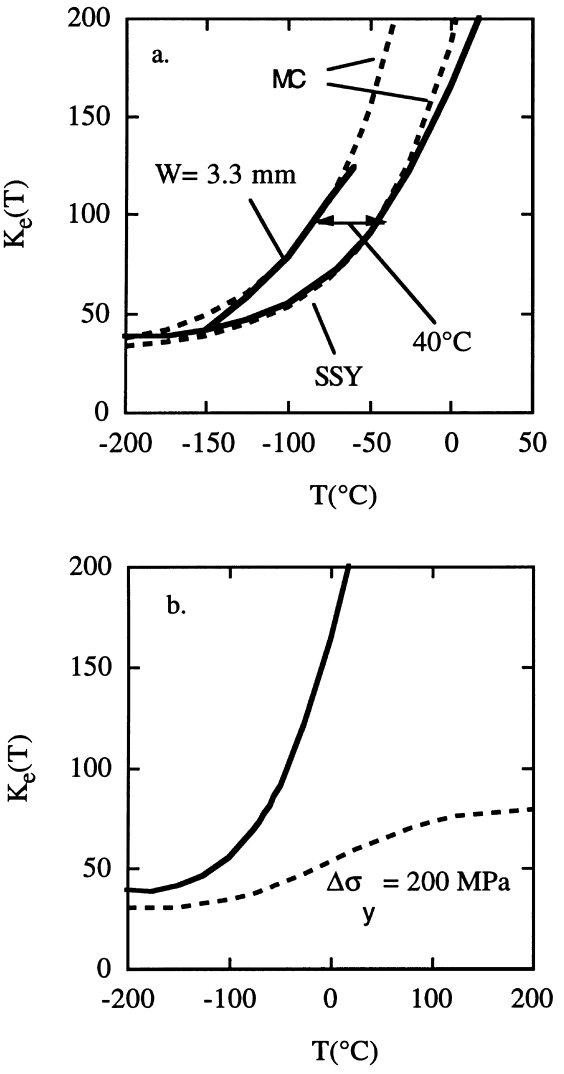

Fig. 3. (a) $K_{Jc/e}(T)$ curves computed from Eqs. (2a)–(2c) and (3a) and (3b) for SSY and a subsized specimen geometry; (b) the corresponding predicted $K_{Jc}(T)$ for $\Delta\sigma_y = 200$ MPa for a constant $\sigma^* = 2080$ MPa.

In spite of its general success, the σ^*–A^* model does not explain why the $K_{Jc}(T)$ curves for different steels, with a wide range of microstructures, strength levels and T_0, appear to have a similar MC-type shape. In particular, the constant σ^*–A^* model predicts a significant reduction in the slope of the $K_{Jc}(T)$ curves in the transition at high T_0. Such reductions have not been

generally observed, including cases with high T_0 caused by irradiation hardening. The layover in the $K_{Jc}(T)$ curve due to hardening is illustrated by the dashed line in Fig. 3(b), where the nominal $\sigma_y(T)$ has been replaced by $\sigma_y(T) + 200$ MPa. The layover is simply a consequence of the decreasing temperature dependence of σ_y (and flow stress) with increasing temperature. Thus we must seek a fundamental explanation for the relative insensitivity of the toughness-temperature curve shape.

Perhaps the most general and fundamental explanation is that σ^* increases with temperature due to a corresponding increase in the intrinsic K_{micro} (Eq. (1)) of the metal matrix.

3. A σ^*–A^* $K_{Jc}(T)$ model and microarrest toughness

As noted above, σ^*–A^* are usually assumed to be independent of temperature and strain rate as well as the fine scale features that have an important effect on the constitutive properties. Since A^* primarily depends on the coarse-scale trigger particle microstructure, it is reasonable to assume that it is constant within the framework of RKR-type models. Information on σ^* come from blunt notch tests, where the high stress field sampling volume is sufficiently large so that cleavage is controlled by the peak tensile stress. Most data show constant σ^*, or small decreases or increases with increasing temperature [13,14,16–18].

A corollary to a constant σ^* is that the inherent metal matrix K_{micro} is also temperature independent. Clearly, at sufficiently high temperatures, above an intrinsic ferrite brittle-to-ductile transition (BDT), this is not the case. Significant fundamental research has been devoted to the BDT, spawning a number of different models and concepts [19–22]. The BDT criterion has usually been posed as conditions that allow an atomically sharp crack to extend by brittle cleavage when the fields at its tip exceed the cohesive atomic bonding strength of the material *prior* to the emission of a dislocation. However, dislocation emission blunts the microcrack and locally lowers (shields) the crack tip stress fields. Thus if a dislocation is emitted, the fracture is deemed to be ductile. In recent years, this so-called Rice–Thompson [19] criterion has been extended to reflect more realistic physics, including allowing the possibility of cleavage after significant dislocation emission and nano-blunting [20–22]. Multiple dislocation emission and nano-blunting generally occur, resulting in an evolving dislocation structure in the vicinity of the microcrack tip. This structure locally strengthens the material, reducing subsequent dislocation emission rates and velocities. The dynamic evolution results in microcrack extension by the decohesion-cleavage mechanism if the dislocation structure ultimately prevents subsequent local plastic deformation and further nano-blunting. The corresponding K_{micro} is sensitive to the dislocation mobility, hence, to temperature and strain rates. Mobility is primarily controlled by the thermally activated lattice Peierl's stress. Rather than an abrupt BDT, K_{micro}, increases gradually with temperature.

Detailed multi-scale modeling studies and fundamental experiments are underway to refine and quantify the K_{micro} models. However, a further discussion of this topic is beyond the scope of this study. Rather, Eq. (2a)–(2c) is used to derive a $\sigma^*(T)$ that provides: (a) an MC shape over a wide range of T_0; and (b) observed $K_{Jc}(T)$ curve temperature shifts ($\Delta T_{\phi t}$) as a function of irradiation hardening, $\Delta\sigma_y$. We again assume a simple power-law uniaxial stress–strain model with $n = 0.1$, modified to allow for a no-strain hardening regime at low strains ($\varepsilon_y < \varepsilon < \varepsilon_\lambda$) observed following irradiation.

$$\begin{aligned} &\varepsilon = \varepsilon_y \sigma/\sigma_y, \quad \varepsilon < \varepsilon_y, \\ &\sigma = \sigma_y, \quad \varepsilon_y < \varepsilon < \varepsilon_\lambda, \\ &(\varepsilon - \varepsilon_y)/\varepsilon_y = (\sigma/\sigma_y)^{1/n}, \quad \varepsilon > \varepsilon_\lambda, \\ &\sigma_\psi = E\varepsilon_\psi, \quad \sigma_o/E = 0.0035. \end{aligned} \tag{4}$$

Requiring adherence to universal MC shapes and the observed $\Delta T_{\phi t}$ versus $\Delta\sigma_y$ relations, places significant constraints on fitting $\sigma^*(T)$–A^*. The A^* was primarily fit to the lower shelf toughness. Piecewise linear segments were used to provide an iterative 'eyeball' fit for $\sigma^*(T)$.

The results of this exercise are shown in Fig. 4 for $A^* = 10^{-8}$ m^2. Fig. 4(a) shows the fitted $\sigma^*(T)$ (divided by 20 for purposes of scaling) as the thick, longer dashed line; the unirradiated $\sigma_y(T)$ curve (divided by 5.7) is shown as the thick, shorter dashed line. The solid lines in Fig. 4(a) are the $K_{Jc}(T)$ curves predicted by Eqs. (2a)–(2c) for σ_y (MPa) and ε_λ, respectively, of: 0 and 0, 100 and 0.005, 200 and 0.01 and 300 and 0.02. The thinner, dashed lines are RPV MCs indexed at the same 100 MPa $\sqrt{m}$–temperature as the model predictions. Fig. 4(b) compares the corresponding predicted $\Delta T_{\phi t}$ versus $\Delta\sigma_y$ relation (dashed line) with experimental data compiled by Sokolov [23] and the least squares fit to this data (solid line).

4. Discussion

The predicted $K_{Jc}(T)$ shapes are not in exact agreement with the MC shape. However, the overall consistency between σ^*–A^* model predictions and observed MC-type behavior is very encouraging. Note, even the modest layover of $K_{Jc}(T)$ at higher $\Delta\sigma_y$ is qualitatively consistent with the data evaluation of Sokolov [23]. However, this consistency neither demonstrates the

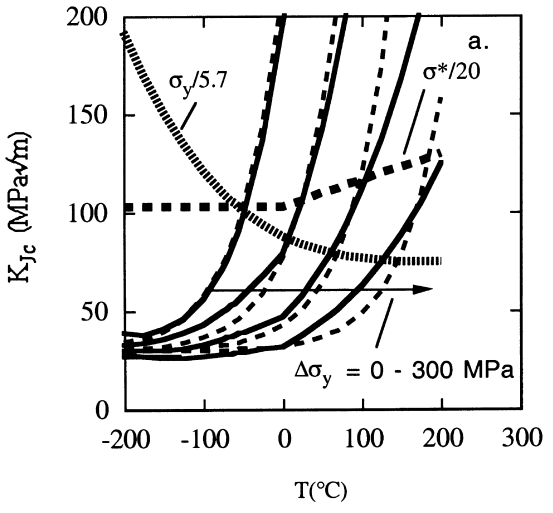

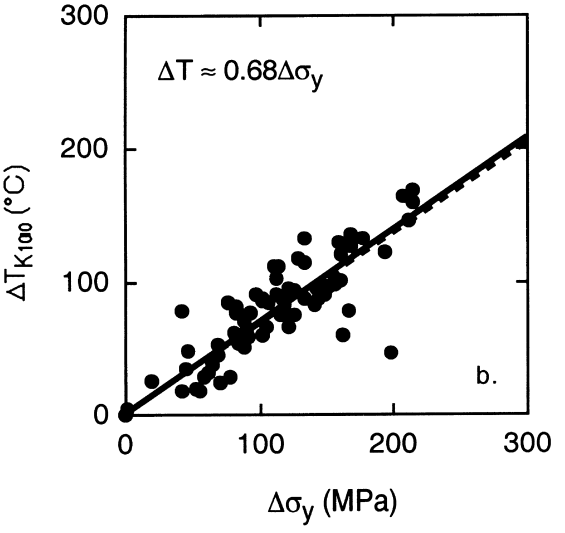

Fig. 4. (a) Predicted vs MC shapes for fitted $\sigma^*(T)/A^*$; (b) Predicted and measured ΔT_{K100} vs $\Delta\sigma_y$.

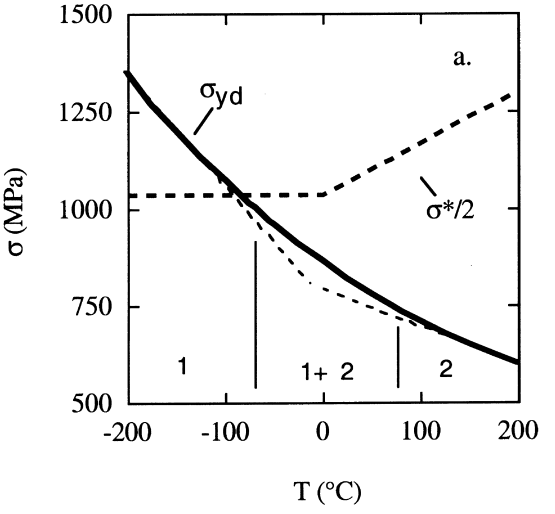

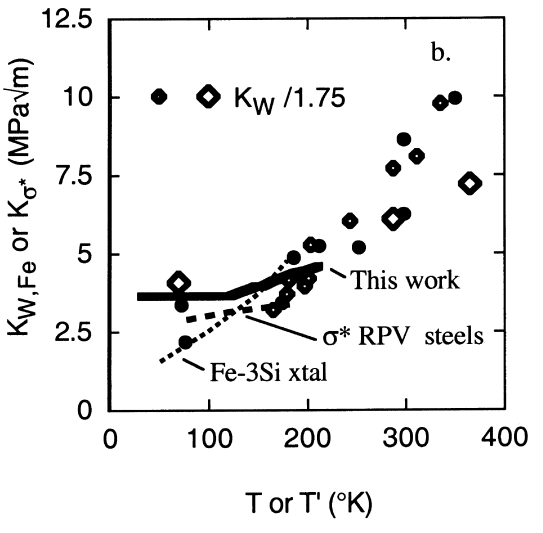

Fig. 5. (a) Comparison of $\sigma^*(T)$ and $\sigma_{yd}(T)$; (b) comparison of $\sigma^*(T)$ (converted to a $K_{\sigma^*}(T)$) with $K_{\sigma^*}(T)$ and $K_{micro}(K)$ data from the literature.

validity of the fitted $\sigma^*(T)$, nor illuminates the underlying source of such behavior.

Support for the hypothesis that the propagation of microcracks from trigger particles is related to the effect of dislocation mobility on K_{micro} is shown in Fig. 5(a), comparing $\sigma^*(T)$ and the dynamic yield stress $\sigma_{yd}(T)$. The σ_{yd}, rather than the static σ_y, is used since the strain rates at the dynamic crack tip are very high. Specifically, we assume that the crack tip strain rate (ε'_d) is 10^8 higher than for static conditions (ε'_s) [24]. The σ_{yd} is given by σ_y at a lower temperature (T' in K) by

$$\sigma_{yd}(T,\varepsilon'_d) = \sigma_y(T',\varepsilon'_s), \tag{5a}$$

where

$$T' = T\left[1 - S^* \ln(\varepsilon'_d/\varepsilon'_s)\right]. \tag{5b}$$

Empirical fits for a variety of steels give $S \approx 0.03$ [25]. In the regime labeled 1, the yield stress is dominated by the lattice Peierls stress, and σ^* is approximately constant. In regime 2 there is a second weaker thermally activated component of σ_y, perhaps associated with interstitial solutes and dislocation interactions. However, the local Peierls contribution is small and σ^* slowly increases.

Fig. 5(b) compares the fitted $\sigma^*(T)$ to recent data in the literature on $\sigma^*(T)$ estimates from blunt notch tests on RPV steels [16]. The RPV steel σ^* data trend (heavy dashed line) is scaled to a corresponding microtoughness

(K_{σ^*}) using $K_{\sigma^*} = \sigma^*(d_{tp})^{1/2}$ (see Eq. (1)) and a nominal trigger particle dimension of $d_{tp} = 1$ μm. Note, while this scaling gives only a very rough estimate of the magnitude of microtoughness, the temperature dependence of K_{σ^*} is of primary interest. In order to account for the dynamic strain rates, the K_{σ^*} curves are plotted on the T' temperature scale. The blunt notch K_{σ^*} for RPV steels increases with temperature at a rate of about 2/3 of that for the fitted $\sigma^*(T)$ found in this work (heavy solid line).

Fig. 5(b) also plots data on the fracture toughness of oriented single crystal iron and tungsten (K_{FeW}). The symbols are measurements reported by Gumbsh for single crystal tungsten with different crack plane/front orientations [26]. The orientation shown by the open diamond symbols has been scaled by a factor of 0.6; and the large open diamonds are pre-deformed for crystals to introduce dislocations. The latter are probably more representative of structural alloys, particularly near trigger particles. The lighter short dashed line is the trend reported for single crystal Fe–3%Si [27]. The single crystal Fe–3%Si data also indicate that $K_{micro}(T)$ increases with temperature at a rate equal to about that of the deformed tungsten crystals, somewhat in excess of the fitted $K_{\sigma^*}(T)$ found in this work.

In summary, the temperature dependence of the empirical $\sigma^*(T)$ derived in this work is reasonably consistent with a limited body of independent data, supporting the hypothesis that K_{micro} increases in the regime where the Peierls contribution to $\sigma_y(T)$ is not significant. An important corollary is that there is no abrupt *intrinsic* ductile-to-brittle transition in bcc crystals and that the cleavage micromode of fracture may persist up to high temperatures, However, if σ_y is low, the macroscopic toughness will be high in this regime.

While space does not permit a detailed discussion, it is noted that the model presented here also provides guidance to alloy design and insight into embrittlement mechanisms. Alloys which minimize the size and volume fraction of trigger particles have a double benefit of lower T_0 and $\Delta T_{\phi t}$. The relationship between $\Delta T_{\phi t}$ and $\Delta\sigma_y$ can be quantified by the model shown in Fig. 4(b). Further, service conditions that result in embrittlement due to solute segregation, or coarse-scale microstructural instabilities (higher temperatures), can be modeled in terms of the corresponding effects on σ^*–A^*. Finally, we believe that there are no unambiguous results regarding the potential role of helium on fast fracture. Several experimental data sets suggest that high helium levels may modestly increase $\Delta T_{\phi t}$ above levels associated with irradiation hardening alone. However, if real, any non-hardening effect of helium should be reflected in a lower σ^* and a higher than normal $\Delta T_{\phi t}/\Delta\sigma_y$ ratio. Such differences have not been reported. Resolution of the 'helium question' will require carefully designed single variable experiments and a comprehensive database which will allow mechanism-based interpretation of the mechanical test data. Finally, the ultimate aim is to include treatment of fracture toughness in a set of hierarchical, multi-scale models to design improved alloys and predict in-service microstructural evolution and consequential property changes.

5. Summary and conclusions

An MC–ΔT method has been proposed as an engineering expedient to enable the use of small specimens in predicting the effects on fast fracture of structural geometry, irradiation and loading rates. However, there are a number of fundamental issues related to the MC that remain to be resolved. Thus, a new model of fracture toughness in the cleavage transition regime has been proposed. The model combines analytical representations of FEA simulations of crack-tip stress–strain fields with a local critical stress-critical stressed area (σ^*–A^*) criterion for cleavage initiation. While this model is clearly a surrogate for more complex underlying physics, it has been very successful in predicting the shape of $K_{Jc}(T)$ curves at low temperatures and treating the effects of geometry and loading rate, as well as irradiation induced Charpy transition temperature shifts. However, the standard constant σ^*–A^* model predicts significant reductions in the slope of $K_{Jc}(T)$ curves following large irradiation-induced $\Delta\sigma_y$. Such shape changes have not been observed. This inconsistency is resolved by incorporating a modest temperature dependence of σ^* in regimes where the lattice friction stress is minimal. The fitted $\sigma^*(T)$ is broadly consistent with an independent body of data in the literature. The model also suggests improved methods of alloy design and a systematic microstructurally based approach to evaluating potential embrittlement processes associated with irradiation hardening, coarse-scale microstructural instabilities and high helium concentrations.

Acknowledgements

The authors thank Professor G.E. Lucas for many helpful discussions. The work was supported by the US Department of Energy and the US Nuclear Regulator Commission.

References

[1] T.L. Anderson, Fracture Mechanics Fundamentals and Applications, 2nd Ed., CRC, Boca Raton, FL, 1995.
[2] G.R. Odette, K. Edsinger, G.E. Lucas, E. Donahue, Small specimen test techniques, ASTM STP-1329 (1998) 298.
[3] ASTM E 1921–97, Standard test method for determination of reference temperature, T_0, for ferritic steels in the

transition range, Annual Book of ASTM Standards 03.01., ASTM (1998) 1068.
[4] R.O. Ritchie, J.F. Knott, J.R. Rice, J. Mech. Phys. Solids 21 (1973) 395.
[5] M. Nevalainen, R.H. Dodds Jr., Int. J. Fract 74 (1995) 131.
[6] K. Edsinger, G.R. Odette, G.E. Lucas, B. Wirth, Effects of Irradiation on Materials 17, ASTM STP 1270 (1996) 670.
[7] G.R. Odette, J. Nucl. Mater. 212–215 (1994) 45.
[8] A.G. Evans, Metall. Trans. A 14A (1983) 1349.
[9] K. Wallin, T. Saario, K. Torronen, Metal Science 18 (1984) 13.
[10] T. Lin, A.G. Evans, R.O. Ritchie, J. Mech. Phys. Solids 34–35 (1986) 477.
[11] J.G. Merkle, K. Wallin, D.E. McCabe, Technical basis for an ASTM standard on determining the reference temperature, T_0, for ferritic steels in the transition range, NUREG/CR-5504 (1998).
[12] G.E. Lucas, H. Yih, G.R. Odette, J. Nucl. Mater. 155–157 (1988) 673.
[13] D.A. Curry, J.F. Knott, Met. Sci. 13 (1979) 341.
[14] G.T. Hahn, Metall. Trans. A 15A (1984) 947.
[15] R.O. Ritchie, W.L. Server, R.A. Wullaert, Metall. Trans. A 15A (1979) 1557.
[16] A. Fabry, Small Specimen Test Techniques, ASTM STP-1329 (1998) 274.
[17] W.W. Gerberich, S.-H. Chen, C.-S. Lee, T. Livne, Metall. Trans. A 18A (1987) 1861.
[18] G.R. Odette, P. M. Lombrozo, R.A. Wullaert, Effects of Irradiation on Materials 11th Symposium, ASTM STP 870 (1985) 841.
[19] J.R. Rice, R. Thompson, Philos. Mag. 15 (1974) 567.
[20] G.E. Beltz, J.R. Rice, C.F. Shih, L. Xia, Acta Mater. (1996) 3943.
[21] D.M. Lipkin, G.E. Beltz, L.L. Fisher, Fracture and Ductile vs Brittle Behavior-Theory, Modeling and Experiment, MRS Symposium Series 536 (1999) 49.
[22] A. Hartmaier, P. Gumbsh, L.L. Fisher, Fracture and Ductile vs Brittle Behavior-Theory, Modeling and Experiment, MRS Symposium Series 536 (1999) 233.
[23] M.A. Sokolov, R.K. Nanstad, Comparison of irradiation-induced shifts of K_{Jc} and Charpy impact toughness for reactor pressure vessel steels, Effects of Radiation on Materials 18th Symposium ASTM STP1325 (1999) 167.
[24] G.T. Hahn, W.F. Flanagan, Dislocation Modeling of Physical Systems, Pergamon, New York, 1980, p. 1.
[25] K. Edsinger, PhD thesis, University of California Santa Barbara, 1995.
[26] P. Gumbsh, J. Riedle, A. Hartmaier, H. Fishmeister, Science 282 (1998) 1293.
[27] R. Pikington, D. Hull, Conf. on Fracture Toughness ISI 20 (1963) 5.